Accepted version of published VoR 10.1016/j.triboint.2017.07.004

Coupling machining and heat treatment to enhance the wear behaviour of an Additive Manufactured Ti6Al4V titanium alloy

Abstract:

The effect of coupling machining with a subsequent heat treatment on the wear behaviour of the Ti6Al4V alloy produced by Electron Beam Melted (EBM) was investigated. Reciprocating sliding wear tests in saline solution and temperature-controlled environment were performed. Results showed that the heat-treated cylinders presented a lower coefficient of friction, less wear rate and higher degree of adhesive wear compared to the not heat-treated ones. It was then demonstrated that coupling machining and heat treatment had a synergistic effect that can be used as an efficient strategy in order to improve the EBM Ti6Al4V wear resistance.

Keywords: sliding contact; coefficient of friction; wear measurement; adhesive wear,

1. Introduction

Titanium alloys are engineering materials interesting for several applications thanks to their high strength-to-weight ratio combined with an excellent corrosion resistance [1,2]. Despite these excellent properties, the main concern for further developments of titanium alloys for biomedical applications is the low wear resistance, whereas, during their service life inside the human body, they are subjected to the significant action of sliding between the articulating surfaces [3,4].

Many research efforts have been devoted to improve the wear resistance of the titanium alloys, as their susceptibility to wear is the main disadvantage that shortens the durability of the implant. The scientific literature reports several records proving that the tribological properties of the titanium alloys are highly dependent on their microstructural characteristics: different treatments resulting in various microstructural features can, indeed, produce tailored mechanical and tribological properties.

Guo et al. [5] studied the effect of alloying the surface of the Ti-5Zr-3Sn-5Mo-15Nb alloy with molybdenum by using a double plasma alloying technique. The obtained microstructure was a dense layer with molybdenum, which extended for several microns below the surface, and was formed replacing the β phase characteristics of the untreated alloy. Such microstructural alteration led to improved tribological properties in terms of lower coefficient of friction and lower wear rate due to the fact that molybdenum layers were harder than the β phase.

Luo et al. [6] applied a thermal oxidation treatment to improve the wear resistance of a titanium alloy devoted to biomedical applications. It was found that a rutile film was formed on the surface of the titanium alloy and a nanohardness improvement was achieved. Tests in bovine serum environment revealed that the treated alloy presented a lower friction coefficient and higher wear resistance than the untreated alloy.

Kao et al. [7] applied a double step technique, composed by a nitriding stage followed by the deposition of a Ti-C:H coating, in order to enhance the tribological properties of the Ti6Al4V alloy subjected to a reciprocating sliding wear regime. The nitriding treatment provoked the Ti6Al4V hardness increase, and, as a consequence, a significant reduction of the friction coefficient and wear rate.

Abdulwahab [8] studied the wear response of the Ti6Al4V alloy subjected to an isothermal treatment, consisting in a solution heat treatment at 960°C followed by an aging at 480°C for different soaking times. The obtained results showed that the heat treated alloy subjected to the longest soaking time presented the best resistance to abrasive wear failure.

Celik et al. [9] applied a multiple-step surface treatment as a strategy to enhance the tribological properties of pure titanium used for dental applications. The titanium surfaces were first coated by plasma nitriding and then CrN-coated thanks to a duplex surface treatment. It was found that the coated surface exhibited better wear properties than the uncoated ones thanks to the increased hardness obtained with the surface treatment.

The processing route to which the material is subjected is another issue that substantially influences the material microstructure and, as a consequence, affects the wear resistance. In the framework of Additive Manufacturing (AM), the Electron Beam Melting (EBM) process appears as an innovative technology to quickly produce Ti6Al4V human implants, which can be customized to the specific patient. The EBM process is classified as a near-net-shape manufacturing process, although semi-finishing and/or finishing machining operations may be needed on functional surfaces [10,11], may have a significant influence on the surface integrity of a workpiece and, as a consequence, on the wear resistance of the Ti6Al4V alloy.

Bruschi et al. [12] studied the influence of the machining parameters and cooling strategies on the AM Ti6Al4V, founding that cryogenic machining affected the machined surface properties in terms of hardness and residual stresses and, therefore, enhanced the wear properties of the titanium alloy. Bertolini et al. [13] investigated the fretting corrosion response of a dry and a cryogenic machined EBM Ti6Al4V. Besides an improved corrosion resistance, they found that the cryogenic machined samples were characterized by an improved wear resistance in terms of coefficient of friction and lower amount of wear rate than the dry ones.

However, in none of the mentioned reports, the effect of a possible heat treatment after semi-finishing machining as a method to influence the wear behavior was evaluated.

To this regard, in this paper, reciprocating sliding wear experiments were conducted on Ti6Al4V samples obtained by EBM, then semi-finishing machined, and finally heat-treated in order to prove if a post-machining heat treatment in the (α+β) domain might have a positive effect on the EBM alloy wear behavior. The EBM Ti6Al4V samples were machined at different cutting speed and feed rate. Then, they were subjected to an (α+β) annealing treatment followed by a 20°C/s cooling stage. Tribological tests in a saline solution and temperature-controlled environment adopting a cylinder-on-plate configuration were performed using the CoCrMo cobalt alloy for the plates and replicating the human body conditions as closely as possible. The obtained results showed that the applied heat treatment was an efficient method to improve the wear resistance of the EBM Ti6Al4V alloy.

2. Experimental

2.1 Material

In the present work, the EBM Ti6Al4V alloy was considered for the tribological tests. The Ti6Al4V samples were obtained from cylindrical billets manufactured through the EBM process using an ARCAM™ Q10 machine. Each billet was manufactured with the symmetry axis parallel to the growing direction, with a diameter of 14 mm and a height of 180 mm. The EBM Ti6Al4V chemical composition and main mechanical properties are reported in Table 1.

The microstructure of the EBM Ti6Al4V in the as-received condition is given in Fig.1: it consists in a α/β dual phase in which the α-phase is composed of fine lamellae, organized in a basket-weave morphology [14].

Table 1: Chemical composition and mechanical properties of the EBM Ti6Al4V in the as-received condition.

Ti6Al4V chemical composition (wt%)							
Al	V	C	Fe	O	N	H	Ti
6	4	0.03	0.1	0.15	0.01	0.003	Bal
Mechanical properties							
E [GPa]		UTS [MPa]		Y [MPa]		HV 0.05	
120		1020		950		335	

These features are the result of the EBM process, namely a rapid solidification and a subsequent annealing due to the temperature of the working zone [15].

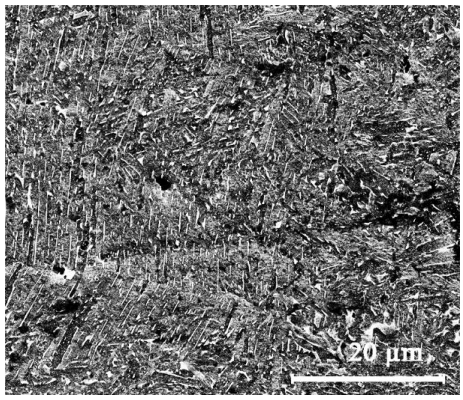

Fig. 1. Microstructure of the EBM Ti6Al4V alloy in the as-received condition.

2.2 Sample preparation and characterization

The machining experimental campaign was conducted on a Mori Seiki™ CNC lathe. The utilized cutting tool insert was a semi-finishing coated tungsten carbide insert DNMG150604SMH13A with a radius of 0.4 mm, mounted on a PDJNR2020K15 tool holder with an approach angle of 93°, both supplied by Sandvik Coromant™. The rake and clearance angles were equal to 7° and 3°, respectively. Both the insert grade and micro-geometry were chosen on the basis of the tool manufacturer's guidelines for machining titanium alloys. Two values of the cutting speed (Vc) and feed rate (f) were chosen, namely 80 and 110 m/min, and 0.1 and 0.2 mm/rev, respectively. The depth of cut (d) was maintained constant and equal to 0.25 mm in

order to achieve a semi-finishing cutting condition. The machining operations were carried out in a regime of full lubrication. Six samples were machined for each condition and three of them was subsequently subjected to the heat treatment.

The heat treatment was conducted for 2 hours in an inert gas atmosphere to prevent the alloy oxidation.

Table 2: Experimental plan for the sample preparation.

Vc (m/min)	f (mm/rev)	Heat treatment
80	0.1	/
80	0.1	✓
110	0.1	/
110	0.1	✓
80	0.2	/
80	0.2	✓
110	0.2	/
110	0.2	✓

The machined Ti6Al4V samples were placed in a furnace that was evacuated and then backfilled with argon before being heated at the treatment temperature of 980°C, in order to be still in the (α+β) domain. The samples were then cooled to room temperature at a cooling rate of 20°C/s.

The summary of the experimental campaign for the sample preparation is reported in Table 2.

Optical microscopy was used for the microstructural analysis, using the Kroll's reagent to etch the polished samples (10 vol% HF and 5 vol% HNO_3 in water). In order to quantify the extent of the globular layer obtained thanks to the heat treatment the following procedure was adopted: the layer thickness was measured from the optical microscopy images recorded at 500X of magnification every 20 μm; the measures were repeated in two different zones of the sample and then the average value was calculated. The same experimental procedure was adopted for the measurement of the extent of the obtained transformed layer below the globular one recording optical microscopy images at 200X of magnification. In the latter case the distance between the two measurements were set at 100 μm.

Vickers micro-hardness measurements were carried out using a Leitz Durimet™ micro-hardness tester with a load of 50 (±0.5) gr for 30 s; three values were recorded for each measurement point and the average value is reported. The hardness measurements were taken every 20 μm from the machined surface to a depth of 100 μm as well as every 50 μm between 100 μm to 400 μm from the machined surface.

Surface roughness measurements were performed using a Sensofar Plu-Neox™ optical 3D profiler with a resolution of less than 20 nm on the optical Z-axis. The average roughness Ra, the mean roughness depth Rz and the maximum height of the profile, Rt, of the turned samples were evaluated along the perpendicular direction with respect to the turning feed marks.

2.3 Wear testing and characterization

The wear resistance of the not-heat treated and heat-treated Ti6Al4V samples was investigated using a Bruker™ tribometer. The tests were performed in a reciprocating wear regime and carried out adopting a cylinder-on-plate configuration in which the cylinder was made to slid against the plate in a linearly reciprocating path. Such type of configuration was selected as it was the most suitable to investigate the behaviour of cylindrical shapes obtained by turning. The material selected for the tribological pair was the cobalt alloy CoCrMo, commonly used as counterpart material of the Ti6Al4V in hip joint replacements.

In order to simulate as closely as possible, the conditions existing in the human body, the tests were performed in a saline solution (0.9% NaCl in distilled water) at a temperature of 37°C ± 2°C. Fig. 2a) shows the tribometer equipped with the used experimental apparatus, while Fig. 2b) and 2c) provide a detailed image of the upper and the lower parts, respectively.

The cylinder is clamped to its holder by means of a screw and they are both connected to a vertical and horizontal translation system. The cylinder holder is mounted on a load cell to acquire the tangential and normal forces during the tests; the normal load sensor provides an in-line feedback control for the vertical movement, which is actively adjusted in order to ensure a constant load during testing. The CoCrMo plate is fixed to the container filled with the saline solution and clamped to it by means of two screws: the container in turn is placed on a plane table controlled by a servo-motor, which allows a linear motion with a speed up to 60 (± 0.5) mm/s. The solution is constantly made recirculate through a pump whose voltage rules its level in the container, keeping it constant for the whole duration of the test. The solution is heated through a commercial resistance heating element placed inside. A thermometer immersed in the solution gives a continuous feedback of the solution actual temperature.

The adopted stroke length was 500 μm and the test frequency was set equal to 10 Hz. A normal load of 7 N was applied in order to reproduce an average contact pressure of 100 MPa; details about the procedure to calculate the latter parameter can be found in a previous paper [13].

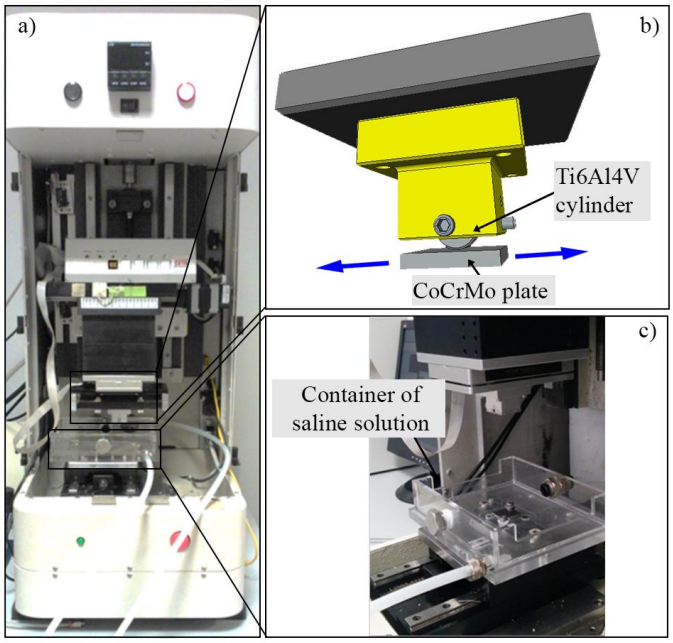

Fig. 2. a) Wear test experimental apparatus; b) schematic representation of the Ti6Al4V cylinder mounted on the cylinder holder; c) detail of the CoCrMo plate fixed inside the container of the saline solution.

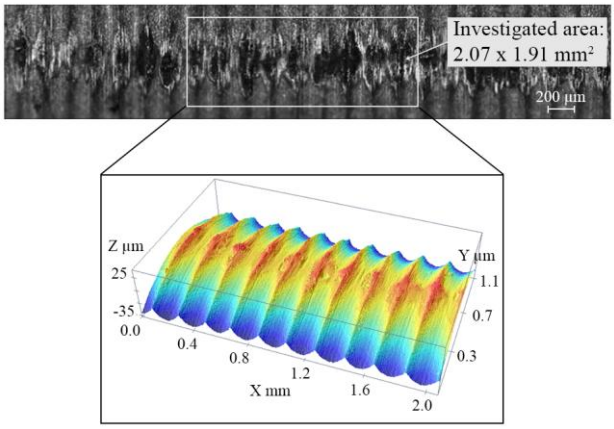

Fig. 3. Schematic image which show where the measurement of the wear volume took place. Images refer to the heat treated Ti6Al4V sample machined at Vc= 80 m/min and f= 0.2 mm/rev.

It is worth to underline that the aforementioned value of the normal load was set in accordance with the work of Zhang et al. [16] who studied from the tribological point of view the stem-head hip connections in the same configuration of the one adopted in this study. Each test lasted 10000 cycles and was repeated three times in order to assure the results repeatability.

Wear characterization after sliding tests was carried out by using two different strategies, namely a 3D profiler analysis and an images analysis procedure based on the BSED-SEM photos. The mentioned characterization techniques were used in order to quantitatively evaluate as much accurately as possible the amount of abrasive and adhesive wear to the overall wear process.

The 3D profiler analysis was used to assess the total wear volume thanks to a procedure that made use of the Nikon 20X confocal objective of the Sensofar Plu-Neox™ optical 3D profiler. As can be seen from Fig. 3,

the scanned area consisted in a rectangle of a width of 2.07 mm and a height of 1.19 mm; the latter value is higher than the scar width but was chosen in order to assure the measurement of a certain amount of undeformed surface.

The measurement width value represents the best compromise between the time of acquisition and the need of acquiring as much worn surface as possible. The acquired area was placed at the center of the wear scar, which was the zone affected by the maximum pressure, thanks to the preliminary positioning step performed using the 10X confocal objective. The acquired z range was fixed to 100 µm constant in all the measurements. Every 500 µm, the wear tracks were analyzed and the average cross section calculated. The latter was then multiplied by the wear track length in order to assess the wear volume.

The worn surface was then examined using a FEI quanta 450™ Scanning Electron Microscope (SEM) equipped with the Everhart-Thornley (ETD) and Backscattered Electron (BSED) detectors. The Energy Dispersive x-ray Spectrometry (EDS) analysis was carried out to identify the surface chemical composition after wear testing.

The amount of adhesive wear was evaluated using an images analysis procedure based on the BSED-SEM photos: a total of three BSED images were first acquired at the center of the wear track and at a distance of ± 1 mm from the center at a magnification of 500X; afterwards, these images were binarized using the ImageJ™ software, and, finally, the number of pixels associated to the black and white areas was measured using the same software, in order to evaluate the amount of adhered material and the amount of the underlying Ti6Al4V alloy, respectively. The binarized images were then post-processed using Matlab™ software in order to get false color images for enhancing the impact visual comprehension.

Fig. 4 schematically shows how the employed characterization techniques contributed to the understanding of the wear phenomenon.

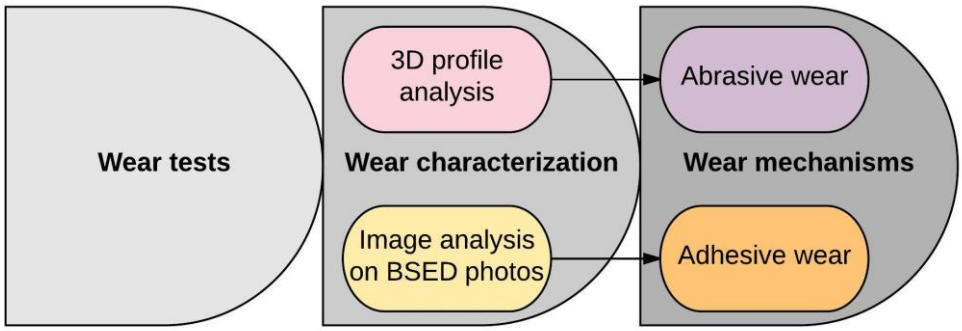

Fig. 4. Flow chart showing the different characterization techniques for the understanding of the wear phenomena

3. Results

3.1 Characterization after machining and heat treatment

Fig. 5 shows the microstructure of the cross section below the surface of two Ti6Al4V samples, one just machined at Vc= 110 m/min and f=0.2 mm/rev, and the other machined using the same parameters and then heat-treated. Similar microstructures were obtained in the case of the other cutting conditions and for this reason they are not reported. Fig. 5A clearly shows that the machining operation induced material alterations below the machined surface: the material was heavily deformed along the cutting speed direction, as demonstrated by the presence of elongated lamellae towards the machining direction. A completely different microstructure is visible for the heat-treated sample shown in Fig. 5B: a sub-surface globular layer was formed, while, under such layer, a transformed layer is present, consisting in α phase and a certain amount of α' martensite with a needle-like morphology with β phase grain boundaries barely visible (magnified SEM images are shown in Fig. 6). The formation of α' martensite is a consequence of the applied cooling rate during the heat treatment, namely 20 C°/s, which is the lowest cooling rate required to obtain a martensitic structure in Ti6Al4V [17].

The change of the α phase from a lamellar to a equiaxed morphology in the sub-surface layer is instead a consequence of the deformation induced by the machining process, which is maximum close to the machined surface, favouring the mechanism of breaking up the alpha lamellae into globular grains [18].

The thickness measures of the transformed and globular layers are reported in Table 3. The thickness of the globular layer is approximately 5 μm for all the samples, regardless the applied cutting parameters.

On the contrary, the thickness of the transformed layer appears is more influenced by the cutting parameters: a higher cutting speed induced a thicker transformed layer as well as the highest the feed rate the thickest the transformed layer, but to a less extent.

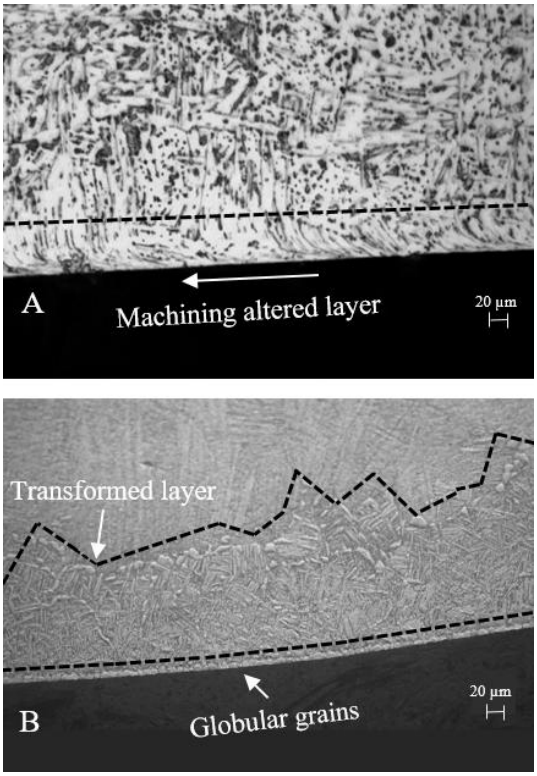

Fig. 5. A) Microstructure of the Ti6Al4V sample machined at Vc=0.2 m/min and f=0.2 mm/rev), B) microstructure of the Ti6Al4V sample machined at Vc=0.2 m/min and f=0.2 mm/rev and then heat-treated.

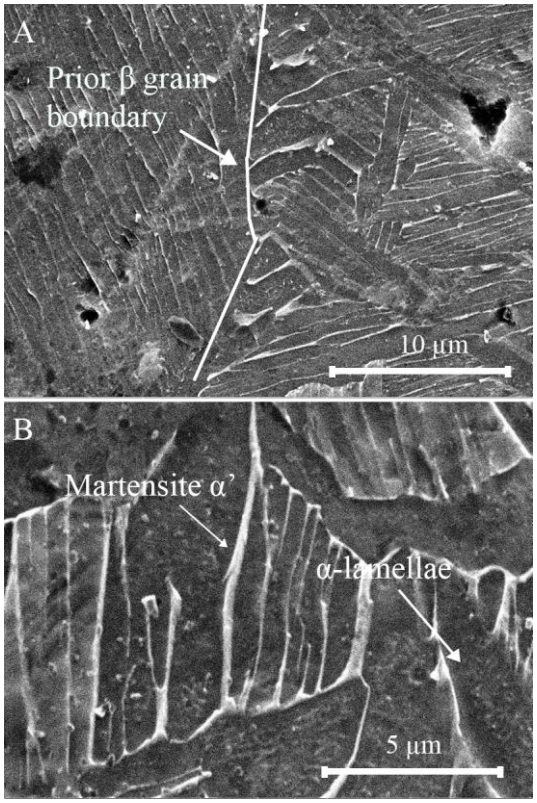

Fig. 6. A) SEM images of the Ti6Al4V sample of Fig. 5B at 10000X; B) SEM images of the Ti6Al4V sample of Fig. 5B at 20000X.

Table 3: Thickness of the globular and transformed layers in the heat-treated Ti6Al4V samples.

Vc (m/min)	f (mm/rev)	Globular layer (µm)	Transformed layer (µm)
80	0.1	5 ± 0.6	122 ± 14
110	0.1	5.1 ± 1	195 ± 18
80	0.2	4.9 ± 1	129 ± 11
110	0.2	4.5 ± 0.8	211 ± 36

The effect of the heat treatment after machining process on the material hardness is shown in Fig. 7. Being the cutting speed the parameter mostly affecting the microstructure of the samples after the heat treatment, the hardness was plotted at a fixed value of the feed rate.

The results clearly show that the heat treatment allows reaching a higher hardness below the machined surface in all the testing conditions compared to the not heat-treated samples. This is due to the presence of the fine martensitic plates with a substructure containing dislocations and stacking faults defects [17]. In particular, a micro-hardness increment up to 28% was measured compared to the bulk value indicated in Table 1. It is worth to underline that the reported hardness values do not refer to the globular grain layer whose extension is lower than the distance of the first recorded hardness point.

The effect of the machining parameters and heat treatment on the surface roughness parameters is reported in Table 4. The obtained results confirm that Ra was influenced only by the feed rate: a higher feed rate induced rougher surfaces, whereas a clear trend for the other investigated process parameters could not be identified.

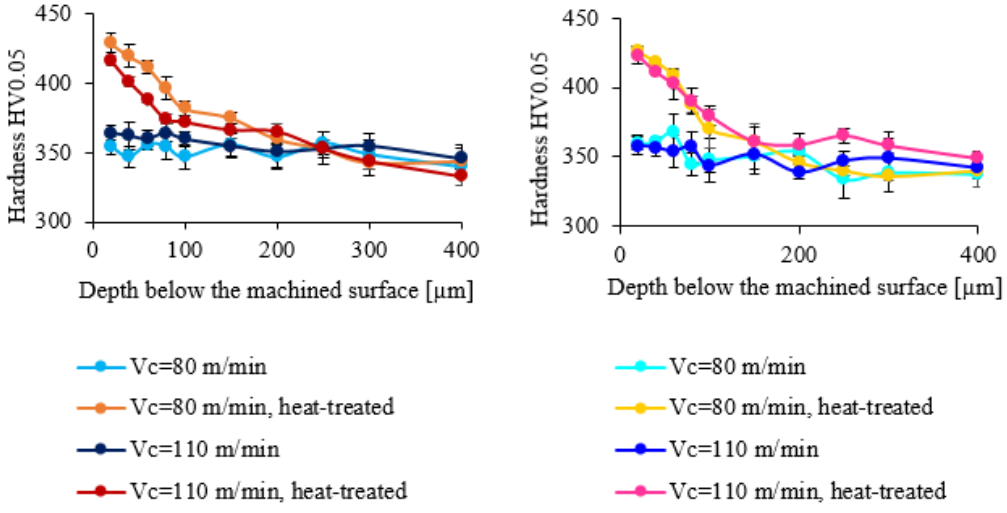

Fig. 7. Micro-hardness profiles below the surface of the Ti6Al4V samples machined at f= 0.1 mm/rev (on the left) and 0.2 mm/rev (on the right); results from both not heat-treated and heat-treated samples are reported.

Table 4: Ra, Rt and Rz values of the Ti6Al4V cylinders as a function of the cutting parameters and heat treatment.

Vc (m/min)	f (mm/rev)	Heat treatment	Ra (µm)	Rz (µm)	Rt (µm)
80	0.1	/	0.965 ± 0.02	4.326 ± 0.17	4.017 ± 0.20
80	0.1	√	0.857 ± 0.03	4.063 ± 0.25	4.443 ± 0.26
110	0.1	/	0.844 ± 0.06	3.675 ± 0.10	4.134 ± 0.16
110	0.1	√	0.842 ± 0.01	3.961 ± 0.13	4.721 ± 0.33
80	0.2	/	2.512 ± 0.02	10.191 ± 0.12	11.075 ± 0.49
80	0.2	√	2.352 ± 0.02	10.291 ± 0.30	12.161 ± 0.52
110	0.2	/	2.262 ± 0.02	9.481 ± 0.21	10.228 ± 0.50
110	0.2	√	2.494 ± 0.04	10.442 ± 0.28	11.495 ± 0.85

Again, both Rz and Rt were primarily influenced by the feed rate: the adoption of feed rate equal to 0.2 mm/rev led to an increase of the Rt and Rz values. A slight increase of the Rz and Rt values was also induced by the heat treatment, with a more pronounced effect using a feed rate of 0.2 mm/rev. The appearance of the 3D topographies reported on Fig. 8 can be explained by the growth of the surface oxide due to the treatment temperature: in fact, the surfaces after heat treatment appear less smooth than the machined ones.

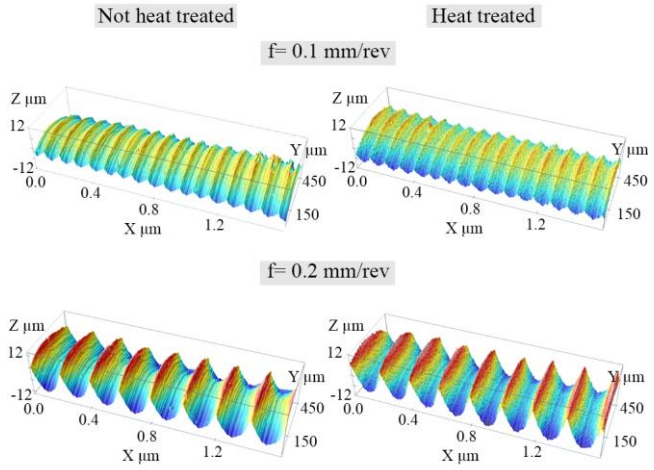

Fig. 8. 3D topographies of the Ti6Al4V samples machined at Vc= 110 m/min.

3.2 Friction analysis

The steady-state values of the Coefficient Of Friction (COF) measured during the wear tests are shown in Fig. 9. The heat-treated samples always present lower COF compared to the not heat-treated ones: this behaviour can be ascribed to the enhanced hardness of the sub-surface layer (for sake of comparison Fig. 9 reports also the relative sub-surface hardness values). In general, the higher the feed rate the higher the COF, whereas the higher the cutting speed the lower the COF. Although there are no general relationships between the trends of the friction coefficient and the specific wear rate, a lower friction coefficient may contribute to a lower wear rate due to a smaller shear force and a lower contact temperature under the same condition [19].

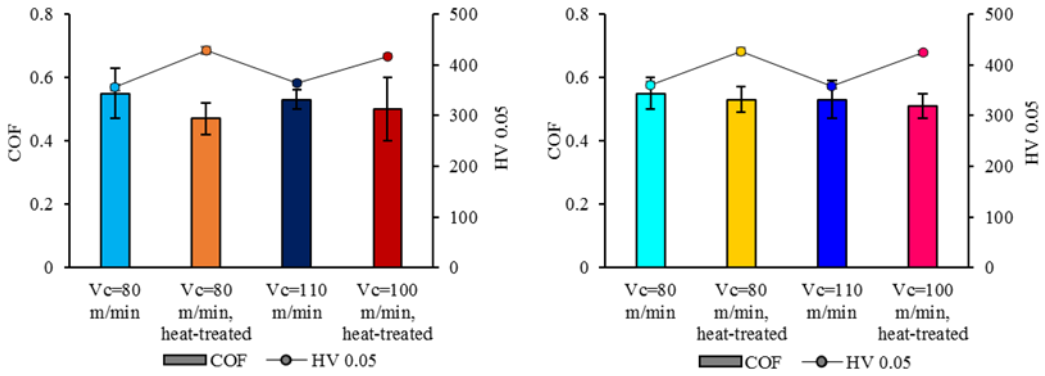

Fig. 9. Average steady state COF and hardness measured at a distance of 20 μm from the surface of the Ti6Al4V samples machined at a f= 0.1 mm/rev (on the left) and 0.2 mm/rev (on the right); results from both not heat-treated and heat-treated samples are reported.

3.3 Wear analysis

Table 5 shows the wear volume values calculated with the procedure described in Section 2.3.

The wear resistance of the non-heat treated samples is much lower than that of the heat treated ones. As can be seen from the wear results, the wear loss of the just machined Ti6Al4V is more than double than that of the heat treated alloy, regardless of the cutting parameters. If we compare the heat treated and not heat treated samples machined with f=0.1 mm/rev and Vc=80 m/min and f=0.2 mm/rev and Vc=110 m/min, the differences reach an order of magnitude. These evidences may be expected since the heat treated samples exhibit higher micro-hardness compared to the not heat treated ones. According to the Archard's law, the volumetric loss of the material is inversely proportional to the hardness value of the material [20]. This implies that the higher the material hardness the smaller the volume loss. The heat treated and not heat treated alloy exhibits significant difference in the hardness values, so that the experimental sliding wear data confirm the Archard's law prediction. Moreover, these results are in accordance with the fact that the heat treated samples were characterized by lower coefficient of friction, as evidenced in Fig. 9. The presence of a martensitic microstructure close to the surface enhanced the wear resistance since it was characterized by a higher hardness compared to the bulk microstructure.

These results are in close agreement with the ones found by Cvijovic et al. [21], who proved that the Ti6Al4V ELI, water quenched from 1000°C, was characterized by a lower wear rate compared to other microstructural conditions thanks to the improved mechanical properties attributed to the martensitic microstructure.

Focusing on the other process parameters, a defined trend could not be found, even if there was a slight influence of the cutting speed when adopting a feed rate of 0.2 mm/rev: a higher cutting speed seemed to be beneficial in terms of reduced wear rate.

The negligible influence of the cutting speed on wear behaviour can be explained by the fact that it did not alter the microstructure as did the heat treatment, but it just influenced the layer extension. As in the sliding process only the surface layer was involved, the main differences can be then ascribed to the microstructure.

Table 5: Average wear volume of the Ti6Al4V cylinders as a function of the cutting parameters and heat treatment.

Vc (m/min)	f (mm/rev)	Heat treatment	Wear volume ($*10^{-3}mm^3$)
80	0.1	/	7.6 ± 1
80	0.1	✓	0.5 ± 0.8
110	0.1	/	3.8 ± 2
110	0.1	✓	1.5 ± 1
80	0.2	/	7.6 ± 3
80	0.2	✓	1.7 ± 1
110	0.2	/	2.9 ± 1.5
110	0.2	✓	0.8 ± 1.3

The SEM observations of the worn surfaces confirmed the above reported results.

Figs. 10 and 11 show the SEM micrographs of the Ti6Al4V scratched surfaces after the wear tests. The figures compare the Secondary Electron (SE) and Backscattered (BSED) detectors images recorded for each sample. The SE images are representative of the topography of the worn surfaces and evidences of abrasion wear can be detected in all tested specimens. Abrasion wear refers to the ploughing phenomena that takes places at the contact interface between two surfaces. As a result of ploughing, a certain volume of surface material is removed and an abrasive groove is formed on the weaker surface [22]. In the present study, continuous sliding marks with plastically deformed grooves and ridges are seen on the wear tracks independently of the testing condition. Similar evidences to those found in this study were reported in [23], where the Ti6Al4V wear characterization was carried out after sliding wear, and surfaces covered with narrow but long grooves formed by abrasion and plastic deformation were found.

The extent of ploughing is found to be smaller in the case of the heat-treated Ti6Al4V samples. The depth of the wear grooves depends on the relative hardness of the abrasive with respect to the specimen surface hardness. As the hardness of the heat-treated Ti6Al4V is higher than that of the not heat-treated material, the depth of penetration of the counterpart material in the heat-treated titanium alloy surface is expected to be lower. This results in lower material removal from the surface due to the ploughing action and, therefore, less wear rate.

The SEM analysis also showed that another wear mechanism was operative, namely adhesive wear. In the case of plastic contact between similar materials, the contact interface has an adhesive bonding strength, as a consequence of the cold welding that occurs at the asperity contacts. The tangential movement due to sliding shears these junctions, causing the sheared asperities to come off.

Existence of the flakes removed from the contact surface (clearly visible on Fig. 10 IIa) strongly suggests the occurrence of adhesive wear. During sliding, the contacting asperities experience an incremental plastic deformation, which accumulates during repeated contacts [24]. When a critical value of the accumulated plastic strain is attained, cracks nucleate below the surface and propagate parallel to the surface. As a consequence, flakes of material are detached from the surface by adhesion to the counterpart.

Furthermore, titanium alloys are chemically active and have a high ductility, giving rise to a strong adhesion tendency [15]. Therefore, the adhesive strength of the formed junctions is usually much higher than the Ti6Al4V strength, and such junctions will rupture within the weaker titanium asperities, which accounts for the craters found on the Ti6Al4V worn surface.

This is why, it was decided to analyse the wear scar through the BSED probe in order to obtain information about the surface chemical composition and find out the presence of material from counterpart. In standard BSED images, chemical elements with different atomic number appear with different grey scale colours, while in these ones reported in Figs 10 and Fig. 11 different grey tones are associated with different colour in order to maximize the difference in shade and give an easier understanding of the results.

All the heat-treated samples are characterized by a higher amount of chemical elements different from the base alloy, which are shown in blue colour. The EDS analysis was carried out on those surfaces in order to evaluate the composition of the material present on the wear scars. Fig. 12 clearly shows the presence of Co, Mo, Cr, besides the bulk material elements, which are the elements of the counterpart material, therefore confirming the presence of the adhered layer. Fig. 12 shows also the presence of micro-cracks orthogonal to the sliding direction: the presence of such cracks can be ascribed to aforementioned strong increase of the hardening of the adhered layers during sliding, which may lead to embrittlement phenomena [25]. The hardness of the transferred alloy actually was substantially increased due to the strain hardening effect. Therefore, this hardened layer could be cracked more easily compared to the base alloy.

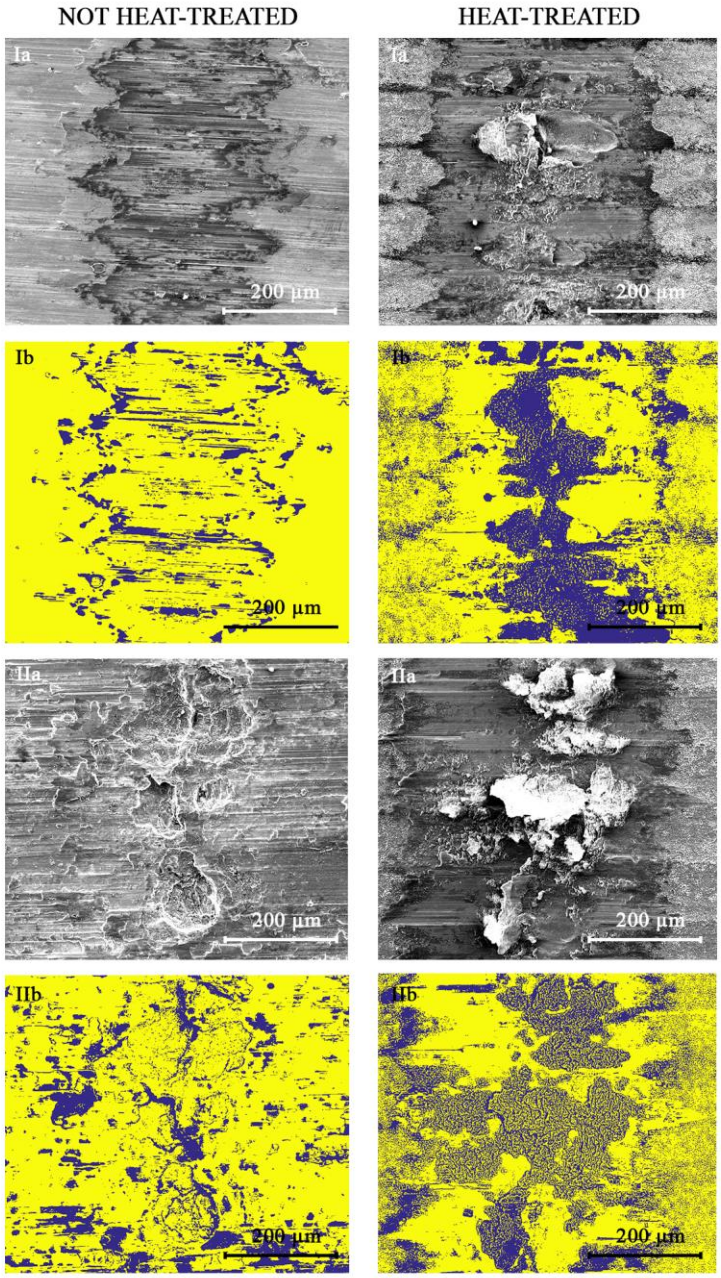

Fig. 10. SEM images of the wear scars on the Ti6Al4V samples machined at f=0.1 mm/rev. Legenda: a) SE images, b) BSED images; I) samples machined at Vc= 80 m/min, II) samples machined at Vc= 110 m/min.

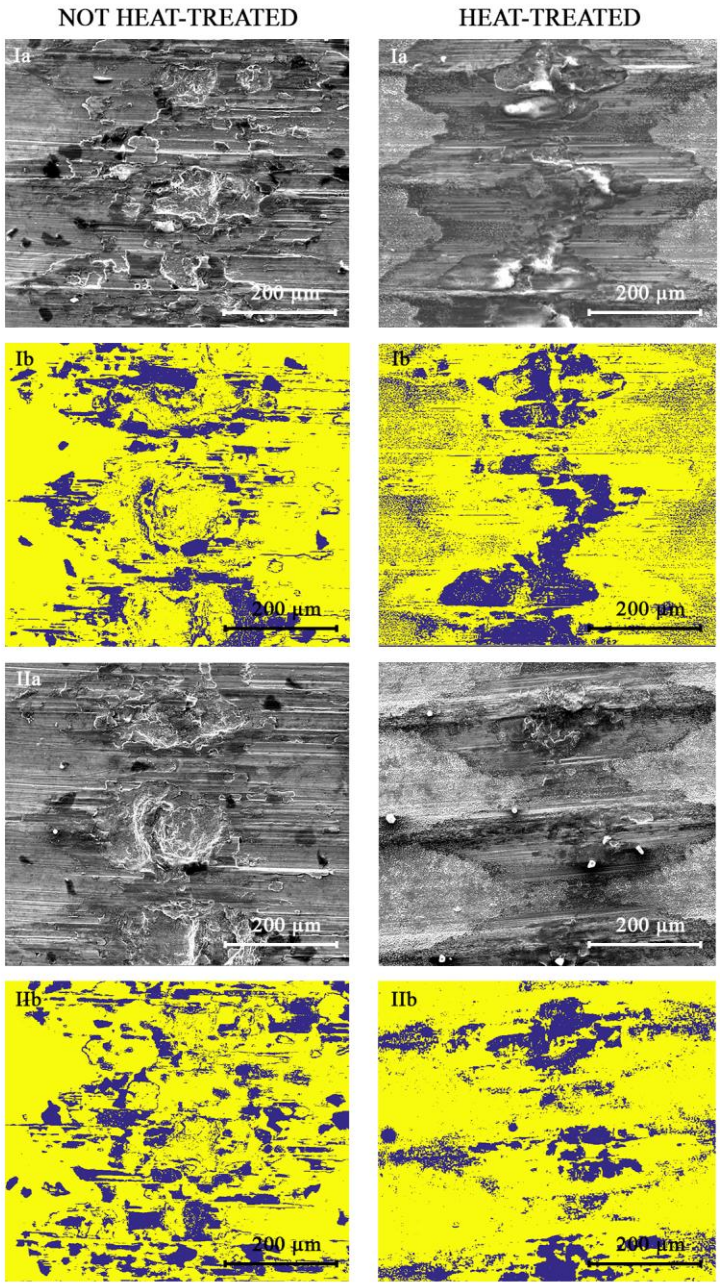

Fig. 11. SEM images of the wear scars on the Ti6Al4V samples machined at f=0.2 mm/rev. Legenda: a) SE images, b) BSED images; I) samples machined at Vc= 80 m/min, II) samples machined at Vc= 110 m/min.

The amount of adhesive layers measured on the Ti6Al4V as a function of the cutting parameters and heat treatment is shown in Fig. 13 with the quantitative data reported in Table 6. In general, the heat-treated samples were characterized by a higher amount of adhesion of the counterpart material. In particular, analysing the location of such adhered layers, a clear difference can be noticed: while for the not heat-treated Ti6Al4V samples the adhered material was limited at the end of the wear track, in the case of the heat-treated samples the counterpart material was placed at the middle of the wear track acting as a barrier for further wear.

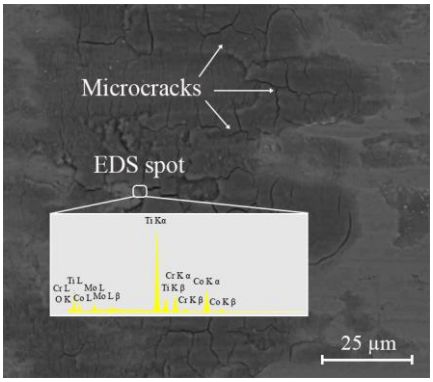

Fig. 12. BSED image of the worn surface of the heat-treated Ti6Al4V sample machined at Vc= 80 m/min and f= 0.1 mm/rev and EDS spectrum of the marked point proving the presence of CoCrMo in the darker area of the BSED image.

As an example, for the heat-treated sample machined at Vc= 80 m/min and f= 0.1 mm/rev, which was characterized by the lowest wear volume, the presence of a patch of adhered layer spread in the centre of the wear scar can be noticed, which can protect the underlying material from further abrasive wear. Similar considerations pertain to all the other heat-treated samples. The fact that adhesive wear occurred at the peaks whereas the abrasive phenomena dominated the valleys region was accordance with the findings in [23].

The development of such layers reduces the material loss since newly formed wear debris particles are recycled into the layers; furthermore, as the wear debris particles are heavily deformed and oxidized as a consequence of the wear testing, these layers are hard and wear-protective [26].

In the case of biomedical applications, the reduction of wear debris is one of the major goal since they are frequently associated with adverse reactions such as osteolysis [27].

On this basis, the presence of adhered layers can be considered beneficial for the Ti6Al4V wear resistance, protecting the surface from further wear and entrapment of wear debris.

Table 6: Average amount of CoCrMo adhered on the Ti6Al4V surface as a function of the cutting parameters and heat treatment.

Vc (m/min)	f (mm/rev)	Heat treatment	Average amount of adhered CoCrMo (%)
80	0.1	/	14 ± 1
80	0.1	✓	30 ± 7
110	0.1	/	21 ± 2
110	0.1	✓	35 ± 4
80	0.2	/	20 ± 3
80	0.2	✓	27 ± 1
110	0.2	/	23 ± 2
110	0.2	✓	27 ± 1

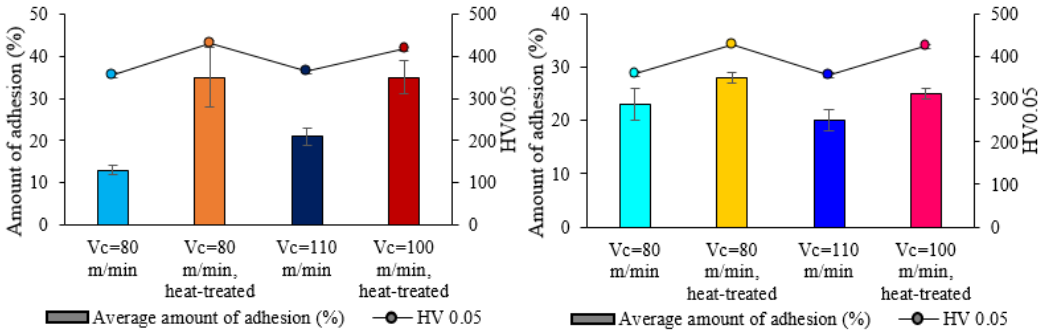

Fig. 13. Amount of CoCrMo adhesion (%) on the Ti6Al4V samples and hardness measured at a distance of 20 µm from the surface of the Ti6Al4V samples machined at f= 0.1 mm/rev (on the left) and 0.2 mm/rev (on the right); results from both not heat-treated and heat-treated samples are reported.

4. Conclusions

The microstructure of the EBM Ti6Al4V titanium alloy was varied coupling a heat treatment with the deformation introduced in the material by a machining operation. Different cutting parameters were applied in order to vary the extent of the altered layers below the machined surface.

The machined and subsequently heat-treated samples showed a very thin layer of globular microstructure just below the machined surface followed by a martensitic structure that extended to several tens of microns below the surface. This change in the microstructure as a consequence of the heat treatment led to an appreciable increase in the samples sub-surface hardness.

Reciprocating sliding tests were carried out in a saline solution at the body temperature with the aim of testing the wear resistance of the not heat-treated and heat-treated Ti6Al4V samples. The wear testing results showed that the heat treatment had a positive effect on the wear behaviour of the heat-treated Ti6Al4V samples. All the heat-treated samples showed lower coefficient of friction and lower wear rate compared to the not heat-treated ones. The main wear mechanism were abrasive and adhesive wear; a higher amount of material adhered from the counterpart characterized the heat treated samples, which could have played as a wear barrier and therefore have limited the abrasive contribution.

Regarding the machining parameters, the cutting speed seemed to play the major role in influencing the amount of altered material during machining, resulting in a higher extent of the microstructural transformed layer. However, these alterations did not lead to an appreciable effect in reducing the wear rate.

The sub-surface hardness had a great influence on the wear behaviour since the sample characterized by the highest hardness near the machined surface showed the best behaviour in terms of coefficient of friction, wear resistance and amount of adhered material.

Based on these findings, coupling the heat treatment with machining was proved to be an efficient method to strengthen the Ti6Al4V wear behaviour and, therefore, increase the durability of the biomedical devices.

This research did not receive any specific grant from funding agencies in the public, commercial, or not-for-profit sectors.

References

[1] Li Y, Yang C, Zhao H, Qu S, Li X, Li Y. New developments of ti-based alloys for biomedical applications. Materials 2014;7:1709–1800.

[2] Popoola API, Phume L, Pityana S, Aigbodion. In-situ formation of laser Ti6Al4V–TiB composite coatings on Ti6Al4V alloy for biomedical application. Surf. Coating Tech 2016; 285:161-170.

[3] Souza CM, Henriques M, Teughels W, Ponthiaux P, Celis JP, Rocha LA, Wear and Corrosion Interactions on Titanium in Oral Environment. Lit Rev, J Bio- TriboCorros 2015;1:1–13.

[4] Balla VK, Soderlind J, Bose S, Bandyopadhyay A, Microstructure, mechanical and wear properties of laser surface melted Ti6Al4V alloy. J Mech Behav Biomed Mater. 2014;32:335–344.

[5] Guo L, Qin L, Kong F, Yi H, Tang B. Applied Surface Science Improving tribological properties of Ti-5Zr-3Sn-5Mo-15Nb alloy by double glow plasma surface alloying. Appl Surf Sci 2016;388:203–211.

[6] Luo Y, Chen W, Tian M, Teng S. Thermal oxidation of Ti6Al4V alloy and its biotribological properties under serum lubrication. Trib Int 2015; 89:67–71.

[7] Kao WH, Su YL, Horng JH, Huang HC, The Tribological Performance of Surface Treated Ti6A14V as Sliding Against Si3N4 Ball and 316L Stainless Steel Cylinder. J Mater. Eng. Perf. 2016;25:5209–5219.

[8] Abdulwahab M, O. Enechukwu, Aigbodion VS. Yaro SA, Mitigation of the Wear Failure of Ti-6Al-4V Dental Biomedical Implant by Isothermal Treatment. J Fail Anal Pre. 2015:15;952–957.

[9] Celik I, Influence of Duplex treatment on structural and tribological properties of commercial pure titanium. High Tem Mater Proc 2017:36;63-68.

[10] Murr LE, Quinones SA, Gaytan SM, Lopez MI, Rodela A, Martinez EY, Hernandez DH, Martinez E, Medina F, Wicker RB. Microstructure and mechanical behavior of Ti-6Al-4V produced by rapid-layer manufacturing, for biomedical applications. J Mech Behav Biomed. Mater 2009;2:20–32.

[11] Murr LE, Esquivel EV, Quinones SA, Gaytan SM, Lopez MI, Martinez EY, Medina F, Hernandez DH, Martinez E, Martinez JL, Stafford SW, Brown DK, Hoppe T, Meyers W, Lindhe U, Wicker RB. Microstructures and mechanical properties of electron beam-rapid manufactured Ti-6Al-4V biomedical prototypes compared to wrought Ti-6Al-4V. Mater Charact 2009;60:96–105.

[12] Bruschi S, Bertolini R, Bordin A, Medea F, Ghiotti A. Influence of the machining parameters and cooling strategies on the wear behavior of wrought and additive manufactured Ti6Al4V for biomedical applications. Tribol Int 2016;102:133–142.

[13] Bertolini R, Bruschi S, Bordin A, Ghiotti A, Pezzato L, Dabalà M. Fretting Corrosion Behavior of Additive Manufactured and Cryogenic-Machined Ti6Al4V for Biomedical Applications. Adv Eng Mater 2016:1–9.

[14] Tan X, Kok Y, Toh WQ, Tan YJ, Descoins M, Mangelinck D, Tor S, Leong KF, Chua CK. Revealing martensitic transformation and α/β interface evolution in electron beam melting Ti-6Al-4V. Nat Publ Gr 2016;1–10.

[15] Bordin A, Bruschi S, Ghiotti A, Bariani PF. Analysis of tool wear in cryogenic machining of additive manufactured Ti6Al4V alloy. Wear 2015;328:89–99.

[16] Zhang T, Harrison NM, McDonnell PF, McHugh PE, Leen SB. A finite element methodology for wear fatigue analysis for modular hip implants. Tribol Int 2013;65:113–27.

[17] Tan X, Kok Y, Tan YJ, Descoins M, Mangelinc D, Tor SB, Leong KF, Chua CK. Graded microstructure and mechanical properties of additive manufactured Ti–6Al–4V via electron beam melting. Acta Biomater 2015;97:1-16.

[18] Ma X, Zeng W, Tian F, Zhou Y. The kinetics of dynamic globularization during hot working of a two phase titanium alloy with starting lamellar microstructure. Ma Sci Eng A 2012;548:6-11.
[19] Chang L, Friedrich K, Y L. Study on the Transfer Film Layer in Sliding Contact Between Polymer Composites and Steel Disks Using Nanoindentation. J Tribol 136 2013;136:1-11.
[20] Archard JF. Contact and Rubbing of Flat Surfaces. J Appl Phy.1953;24:981..
[21] Cvijović Alagić I, Cvijovć Z, Mitrović S, Panić V, Rakin M. Wear and corrosion behaviour of Ti-13Nb-13Zr and Ti-6Al-4V alloys in simulated physiological solution. Corros Sci 2011;53:796–808
[22] B. Bhushan, Introduction to Tribology, John Wiley & Sons, UK, 2013.
[23] Magaziner RS, Jain VK, Mall S, Wear characterization of Ti–6Al–4V under fretting–reciprocating sliding conditions. Wear 2008;264:1002–1014.
[24] Suh NP. Update on the delamination theory of wear. in: D.A. Rigney, editors. Fundamentals of Friction and 1Wear of Materials, ASM, Materials Park, Ohio, USA; 1980, p. 43-71.
[25] Doni Z, Alves AC, Toptan F, Gomes JR, Ramalho A, Buciumeanu M, Palaghian L, Silva FS. Dry sliding and tribocorrosion behaviour of hot pressed CoCrMo biomedical alloy as compared with the cast CoCrMo and Ti6Al4V alloys. Mater Des 2013;52:47–57.
[26] Jiang J, Stack MM. Modelling sliding wear: From dry to wet environments. Wear 2006;261:954–965.
[27] Sansone V, Pagani D, Melato M. The effects on bone cells of metal ions released from orthopaedic implants. A review Clinical Cases in Mineral and Bone Metabolism 2013;10:34-40.